Leaching of Conductive Species:

Implications to Measurements of Electrical Resistivity

R Spragg[1,5], S Jones[2], Y Bu[3],Y Lu[4], D Bentz[2], K Snyder[2], J Weiss[5]

[1]Purdue University, West Lafayette, IN

[2]National Institute of Standards and Technology, Gaithersburg, MD

[3]Twining, Inc., San Diego, CA

[4]Boise State University, Boise, ID

[5]Oregon State University, Corvallis, OR

Abstract

Electrical tests have been used to characterize the microstructure of porous materials, the measured electrical response being determined by the contribution of the microstructure (porosity and tortuosity) and the electrical properties of the solution (conductivity of the pore solution) inside the pores of the material. This study has shown how differences in concentration between the pore solution (i.e., the solution in the pores) and the storage solution surrounding the test specimen leads to significant transport (leaching) of the conductive ionic species between the pore solution and the storage solution. Leaching influences the resistivity of the pore solution, thereby influencing electrical measurements on the bulk material from either a surface or uniaxial bulk resistance test. This paper has three main conclusions: 1.) Leaching of

conductive species does occur with concentration gradients and that a diffusion based approach can be used to estimate the time scale associated with this change. 2.) Leaching of ions in the pore solution can influence resistivity measurements, and the ratio of surface to uniaxial resistivity can be used as a method to assess the presence of leaching and 3.) An estimation of the magnitude of leaching for standardized tests of cementitious materials.

Keywords: electrical properties, resistivity, conductivity, alkali leaching, pore solution, simulation, diffusion; formation factor

1 Introduction

Electrical measurements in cementitious systems are gaining increasing use to quantify the transport properties of concrete mixtures[1–9]. Frequently, electrical resistivity is used to determine the ionic transport properties of concrete as it can be related to the chloride ion diffusion coefficient [10,11]. The diffusion coefficient can be used with service-life prediction models to estimate service life of a concrete element [12–14].

One of the most-often presented equations describing the electrical properties of a fully saturated system is the Nernst-Einstein equation, shown in Equation 1:

$$\frac{\rho_T}{\rho_o} = \frac{D_o}{D} = F = \frac{1}{\phi\beta} \quad [1]$$

where ρ_T is the bulk concrete resistivity that is a measured parameter, ρ_o is the pore solution resistivity discussed in detail below, D_o is the self-diffusion coefficient that describes how a particular ionic species diffuses through a dilute solution and is tabulated for different species for different temperatures [15], D is the bulk concrete diffusion coefficient that describes the diffusion not considering binding or potential effects, F is the formation factor, ϕ is the porosity, and β is the inverse of the tortuosity of the porosity (0 to 1) [10,16].

Equation 1 illustrates that the resistivity of the pore solution, ρ_o, is an important factor when determining the formation factor; it cannot be inferred from bulk resistivity measurements alone. When sealed curing is used in cementitious systems (i.e., when no outside fluid enters or leaves the specimen) the composition of the cementitious materials and the mixture proportions can be used to estimate the pore solution chemistry (species concentrations). This can be used to estimate the pore solution resistivity using a procedure described by Taylor [17] and Snyder et al. [18], and that has also been programmed into a web application by Bentz [19], available at http://concrete.nist.gov/poresolutioncalc.html. Numerous research studies have shown a good correlation between this theoretical approach and experimental values, for a sealed sample, for ordinary portland cement (OPC) concretes, e.g. [11,20–24]. The primary concern with sealed specimens is they are not a saturated system, and Equation 1 is generally applied to a saturated system. However, corrections for non-saturated systems (non air-entrained) have been developed [25].

64 Pore solution measurements on water-cured specimens can exhibit a significant deviation
65 between experimental results and estimates based on the soluble alkalis, e.g. [26]. The web-
66 based model discussed in the preceding paragraph has an option for saturated curing. This option
67 incorporates the effects of saturation by reducing the concentration of the pore solution
68 consistent with additional water being provided to account for the chemical shrinkage, but this
69 approach does not match experimentally obtained results on specimens that are stored under
70 water. This approach does, however, seem to agree with estimates for pore solutions that are
71 expressed from specimens that are sealed cured and then vacuum saturated at time of testing
72 [26]. The authors have hypothesized that this is due to conductive species leaving the pore
73 solution, i.e., leaching, and going into the storage solution. A conceptual illustration of this is
74 shown in Figure 1.
75

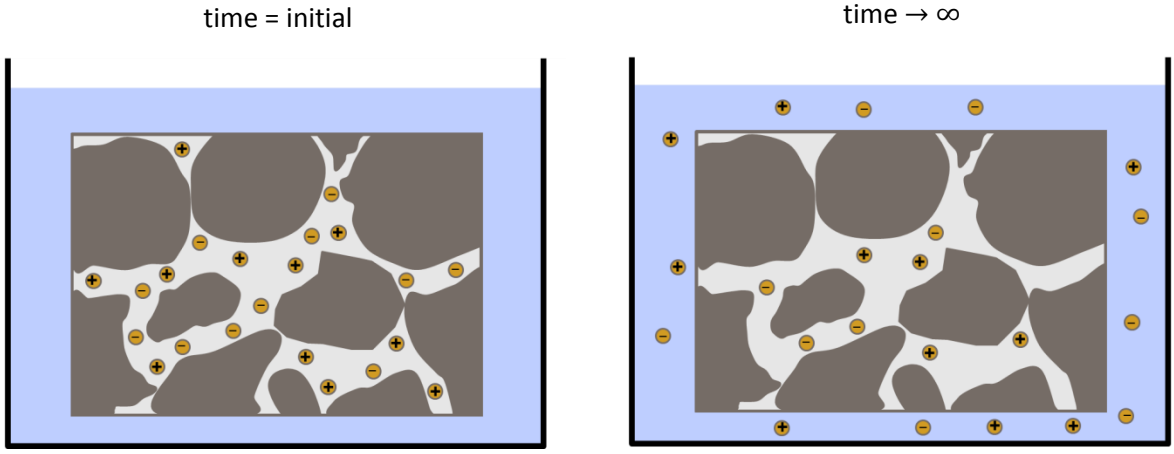

76 ***Figure 1*** *Conceptual illustration of conductive species in the pore solution of a porous material,*
77 *a) where no leaching has occurred and b) after leaching has occurred to equalize the*
78 *concentration differences between the pore and storage solutions.*
79

The likelihood of ionic leaching into the surrounding solution can be evaluated by comparing the concentrations of species within the pore solution and the storage solution. In typical cementitious systems, the pore solution is predominately composed of potassium (K^+), sodium (Na^+), and hydroxides (OH^-) species. An approximate concentration of these ions, $[K^+]+[Na^+]=[OH^-]$, can be around 1.2 mol/L, but the exact value is depends strongly on the mixture characteristics, the chemistry of the cementitious materials, and the curing age [18]. Conversely, the composition of the storage solution is often much lower in terms of the concentration of these ions. Often, a storage solution of saturated lime-water (calcium hydroxide) is suggested [27], in which case the concentration of K^+ and Na^+ is initially low, and that of OH^- is not much higher (approximately 0.05 mol/L). If saturated lime-water is not used, calcium hydroxide leaching can take place which can cause an increase in porosity and alter the microstructure. This equates to a large concentration difference between the high concentration pore solution and the low concentration storage solution, which leads to the leaching of ionic species from the pore solution in the sample.

Alkali leaching has been noticed previously in alkali-silica reaction (ASR) studies, as far back as the 1940s [28]. Blanks and Meissner analyzed the water at the bottom of a bucket containing a specimen undergoing ASR expansion, and noticed that the pH of the solution in the bucket varies quite significantly depending on the alkali content of the cementitious materials being tested. A study by Rogers and Hooton [29] used a series of different curing conditions (number of bars and the presence of wicking material) with the same nominal mixture design and evaluated the equivalent alkalis. Their results showed that the alkali concentration of the sample varies widely.

Famy et al. [30] showed that when storing samples in a humidity of 80 % to 100 %, 80 % of the K^+ ions and 60 % of the Na^+ ions can leach within the first ten days. Leaching has also been discussed by Thomas et al. [31] and Rivard et al. [32]. The reduction in alkalis in a test specimen and an increased concentration in a storage container has also been noted by Muberra and Glasser [33], and in a study by Diamond [34] it has been suggested that alkali leaching is the reason that delayed ettringite is seen in laboratory samples but not field structures.

A study by Spragg et al. [24] has highlighted the impact of storage solution volume on electrical measurements, which has been attributed as an artifact of alkali leaching. In a previous study, a simplified linear mass balance approach was used to estimate the change in pore solution resistivity based upon the change in the resistivity of the storage solution [11].

2 Research Significance

The use of electrical measurements as a method for evaluating the transport properties of cementitious materials requires knowledge of both the measured resistivity of the specimen and the resistivity of the pore solution. If leaching occurs, as illustrated in Figure 1, the pore solution concentration (and resistivity) can change by a significant factor as ions migrate from the specimen into the surrounding storage solution. In a study by Spragg [11], this was shown, for the concrete considered, to be a factor of four. In this paper, experiments and modeling are combined to provide insights into the significance and magnitude of the influence of leaching on electrical properties measured in standardized tests.

3 Experimental Details

The experiments employed in this study were conducted in three phases, and are described in detail below. Phases I and II were used to demonstrate the leaching of the conductive ionic species and to characterize the leaching process through a diffusion-based analysis. The model that was developed did not account for binding, dissolution, or secondary reactions. Phase II was conducted to illustrate the impact of leaching of conductive species from the pore solution on the relationship between measurements performed on different resistivity test geometries. As such, materials whose microstructure was relatively homogeneous and well characterized were used. Furthermore, pore and storage solutions were chosen such that their concentrations could be measured and monitored during the leaching process. Lastly, Phase III used the diffusion simulation model developed in the first two phases as a tool to project the extent of alkali leaching on a standard concrete test cylinder.

3.1 Phase I: Leaching Demonstration and Characterization

The objective of Phase I of this study was to demonstrate that the leaching of conductive species does occur, and that a diffusion approach is able to characterize this process. Experiments for this phase were conducted on thin ceramic disks made from a high-purity aluminum oxide with an average pore size smaller than 0.5 µm and a total porosity of 38 %, based on mass measurements of dry and saturated specimens [35]. The specimens had a diameter of 50 mm

and a thickness of 6 mm. The ceramic was chosen because it had a uniform and non-changing pore structure [35].

The ceramic specimens were vacuum saturated in a solution of potassium chloride (KCl) with a nominal concentration of 7 % KCl by mass. The uniaxial resistivity of the specimens was measured before and after the leaching experiment was conducted.

After vacuum saturation with KCl, the ceramic specimens were measured for electrical resistivity to determine the formation factor, then placed into one of the three following solutions: A) deionized water that is less concentrated than the pore solution; B) 7 % KCl solution by mass, that nominally has the same concentration as the pore solution; or C) 11 % KCl, by mass, which is more concentrated than the pore solution. The storage solution volumes were either twice or five times that of the bulk ceramic disc (11.78 cm^3) that was placed into the container. It is also worth noting that while the storage solution was twice or five times the bulk volume of the ceramic, the storage volume is 5.3 and 13.2 times larger, respectively, than the volume of pore solution originally contained within the disc, as the pore solution can only occupy the porosity of the disks. Testing was conducted in (23 ± 1) °C or (45 ± 1) °C environments; uncertainties represent one standard deviation. A summary is shown in Figure 2, where the chloride ion (Cl-) concentrations are given in units of mol/L.

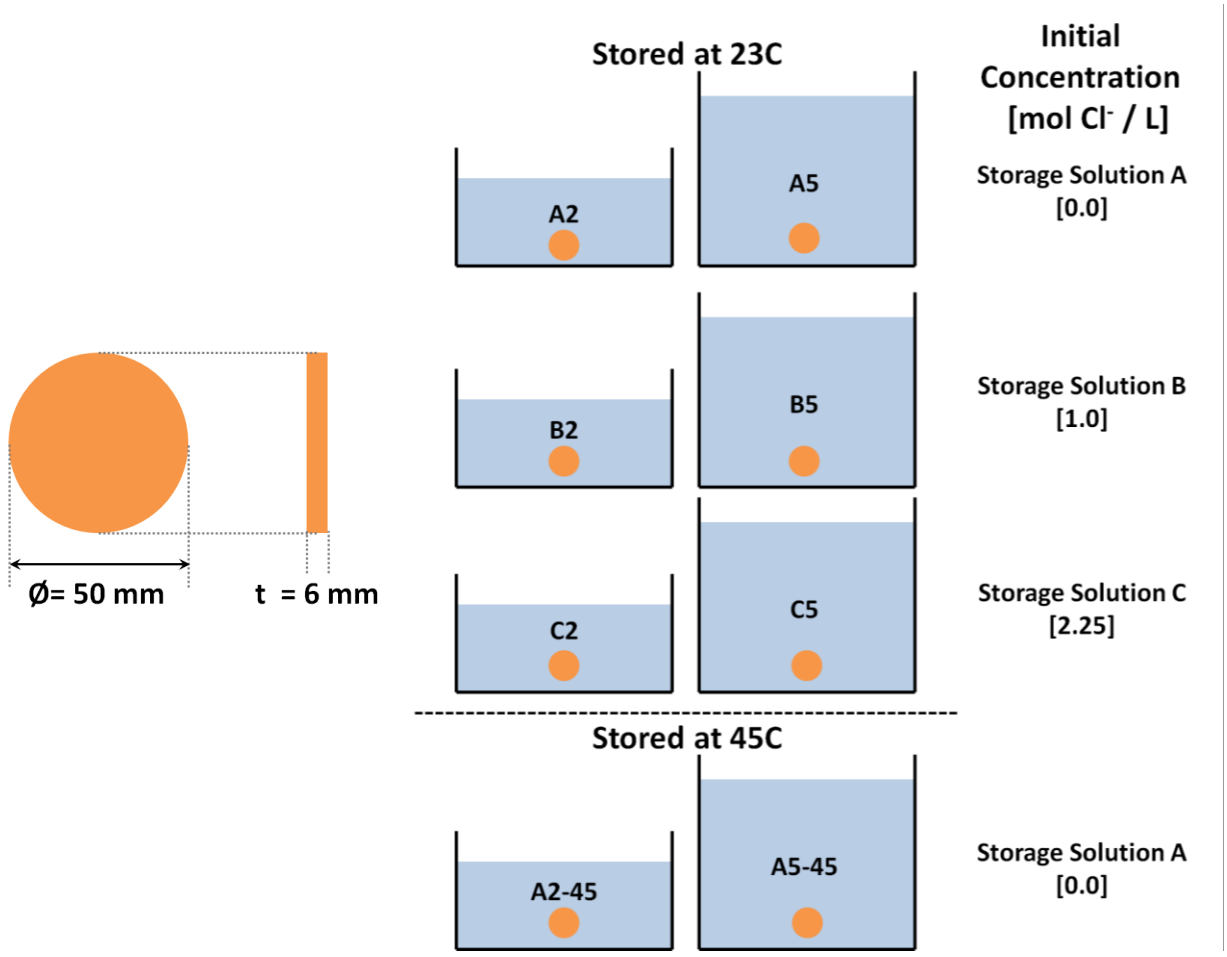

Figure 2 *Experimental Summary of Phase I using ceramic a.) disc geometry and b.) concentration and volume of pore solution where A, B, and C describe the concentration of the initial storage solution (smallest to largest), 2 and 5 represent the volume of solution (twice or five times that of the ceramic sample). The pore solution was the same for all conditions at a chloride concentration of 1.0 mol/L.*

After the ceramic specimens were placed into their respective storage solutions, the concentration of chloride ions in the storage solution was monitored (as a function of time). In

an effort to be consistent, directly before a measurement was taken, the solution was lightly agitated to help to homogenize the solution. A pipette was used to remove 0.5 mL of solution at the selected time. The 0.5 mL of solution was then titrated using an automatic procedure where small increments of $AgNO_3$ solution were added to the solution [36]. $AgNO_3$ reacts with the Cl^- to produce AgCl and will subsequently cause a decrease in the conductivity of the solution. When a sufficient amount of $AgNO_3$ was added such that the conductivity decreases, stoichiometric calculations can be done based upon the amount of $AgNO_3$ added to determine the Cl^- concentration in the sample of storage solution [36].

3.2 Phase II: Impact on Electrical Measurements

The objective of the Phase II study was to show that leaching of ions in the pore solution can influence resistivity measurements and the relationship between measurements obtained using two different resistivity test geometries. For this phase, testing was conducted on cores taken from an Indiana siltstone. Siltstone was chosen because of its consistent pore structure and its availability [16]. The cores were 45 mm in diameter and were approximately 100 mm in length. Their porosity was measured using vacuum saturation and the difference between dry and saturated masses and was calculated to be 11.8 ± 0.2 %, with respect to the dry mass [37].

The siltstone specimens were vacuum saturated with solutions of KCl with nominal concentrations of 5 % and 15 % by mass. The specimens were measured for uniaxial resistivity and surface resistivity, using techniques that have been described previously [22,24]. For surface resistivity, a probe tip spacing of 19 mm was chosen, which is the minimum spacing available for

195 the equipment used in this study. The resistivity was calculated from the measured resistance
196 and a geometrical correction factor suitable for the tip spacing and the dimensions of the
197 cylinder.

198

199 Testing was conducted at (23 ± 1) °C, and the specimens were stored in deionized water having
200 a volume that was four times the volume of the specimen. As the pore solution leached from the
201 siltstone core, surface and uniaxial resistivity measurements were conducted, as well as
202 measurements taken of the concentration of chloride ions in the storage solution. A summary of
203 the experimental program is shown in Figure 3, where the chloride ion concentrations are given
204 in terms of mol/L.

205

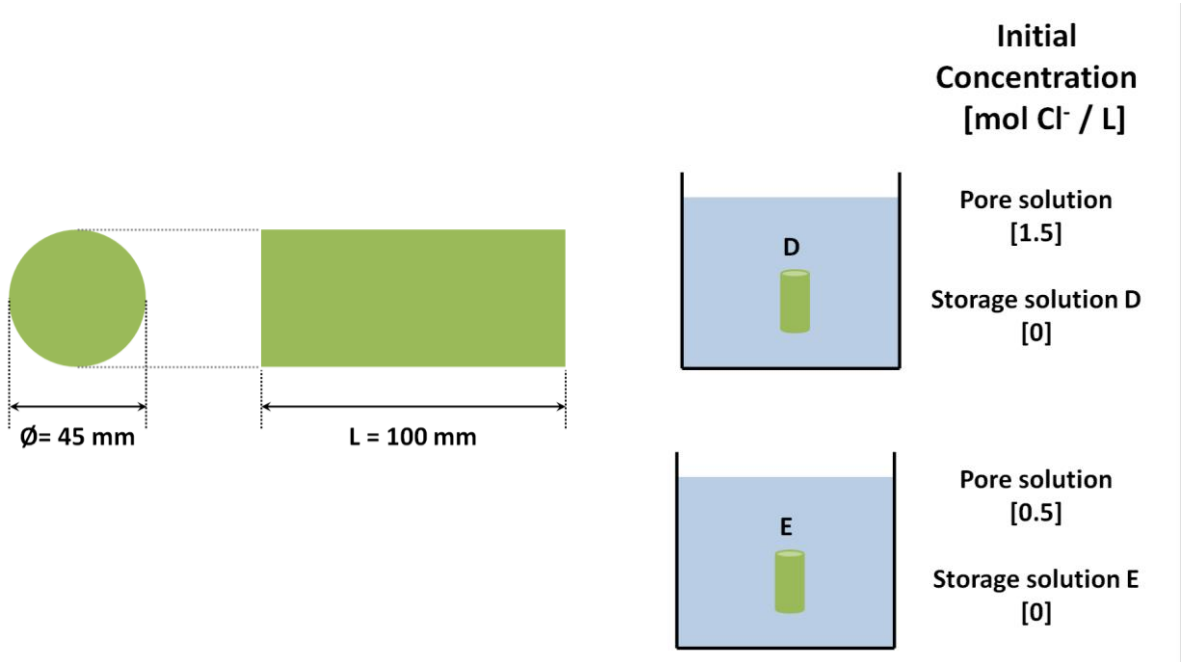

(a) (b)

206 ***Figure 3*** *Experimental Summary of Phase II Siltstone core a.) dimensions and b.) chloride ion*
207 *concentration of pore solution and storage solution in mol/L.*

208

209 ### 3.3 Phase III: Extension to Cementitious Systems

210 Lastly, Phase III of this study provides an estimation of ionic leaching in standard cylindrical
211 concrete test specimen geometries. This phase of the study investigates how leaching might
212 influence electrical measurements on a concrete mixtures.

213

214 ### 3.4 Testing and Simulation

215 Uniaxial resistivity and the resistivity of solutions were experimentally measured using a Solatron
216 1260A Impedance Analyzer[1]. Uniaxial measurements of cylinders and discs were accomplished
217 using plates at the end of the sample and a conductive gel to ensure good electrical contact
218 between the sample and the electrode. The resistivity of the pore solutions and the storage
219 solutions was measured using a small solution conductivity cell, whose geometry factor (0.0125
220 +/- 0.001 m) was determined using a solution of known conductivity. The resistance was tested
221 using a sinusoidal alternating current in the frequency range of 0.1 Hz to 10 MHz, and the bulk
222 resistance was determined from the real component of the impedance at the frequency that
223 minimized the imaginary component of the impedance, as described elsewhere [16,38]. The
224 geometry factor for both the solutions and the specimens was multiplied by the resistance value
225 to determine the resistivity. The resistance measurements have a coefficient of variation of 4.36
226 % [39].

[1] Certain commercial products are identified in this paper to specify the materials used and procedures employed. In no case does such identification imply endorsement or recommendation by the National Institute of Standards and Technology or Purdue University, nor does it indicate that the products are necessarily the best available for the purpose.

Surface resistivity measurements were performed using an equally-spaced four-probe Wenner probe (Proceq Resipod), with an extension kit that allows one to vary the probe spacing. The surface resistivity was determined by Equation 2.

$$\rho = \frac{V}{I} \cdot \frac{2\pi a}{\hat{k}_2} \quad [2]$$

where I is the applied current between the outer probes, V is the measured voltage difference between the inner probes, a is the probe tip spacing (having units of length), and $\hat{k}_2$ is a dimensionless correction factor to account for specimen size and shape. As discussed in detail by Spragg et al. [24] , the correction factor $\hat{k}_2$ was estimated by Morris et al. [40] for cylindrical specimens. Values of $\hat{k}_2$ have been developed for a large range of specimen sizes and probe spacings, and are available in the literature [24,40]. It should be noted that, because resistivity is an intrinsic material property, it is independent of specimen size or measurement methods. Therefore, after applying this correction factor, the ratio of surface to uniaxial resistivities for a homogeneous material should be equal to unity [24].

The solutions used in Phase I and Phase II were potassium chloride (KCl), which was chosen because its concentration, or specifically that of the Cl^-, could easily be measured through the use of an automated titration machine [36]. Moreover, the electro-chemical mobility of K+ and Cl- are nearly equal, so the diffusion of Cl- in a non-reactive porous material will mimic ideal

247 Fickian diffusion. A series of concentration measurements conducted to understand the
248 variability of this measurement method indicate a coefficient of variation of 1.5 %.
249
250 The leaching of ionic species from the pore solution into the surrounding storage solution can be
251 modeled by a two-dimensional, axis-symmetric geometry (shown in Figure 4 consisting of two
252 regions, the disc and the storage solution. By exploiting the cylindrical symmetry, the calculation
253 domain could be limited to the top right quadrant of the system. This reduces both the
254 complexity of the model and the computation time. The domain was discretized using triangular
255 elements with increased density at the boundary of the disc and storage solution to improve
256 solution convergence and precision. A commercial finite element software package (COMSOL
257 Multi-Physics) was used to solve the transport equations for the disc and storage solution. The
258 software allows the user to specify the triangular mesh density, but automatically determines
259 the appropriate element distribution.
260
261 The mathematical model used to describe the transport of chloride ions from the disc to the
262 storage solution can be derived from the continuity equation of a non-deformable, non-reactive
263 porous matrix. A discussion of formulating the continuity equation for diffusion within a porous
264 material can be found elsewhere [41,42] and is reproduced here in Equation 3:
265

$$\phi \frac{\partial c_i}{\partial t} + (\nabla \cdot \boldsymbol{j_i}) = 0 \qquad [3]$$

266

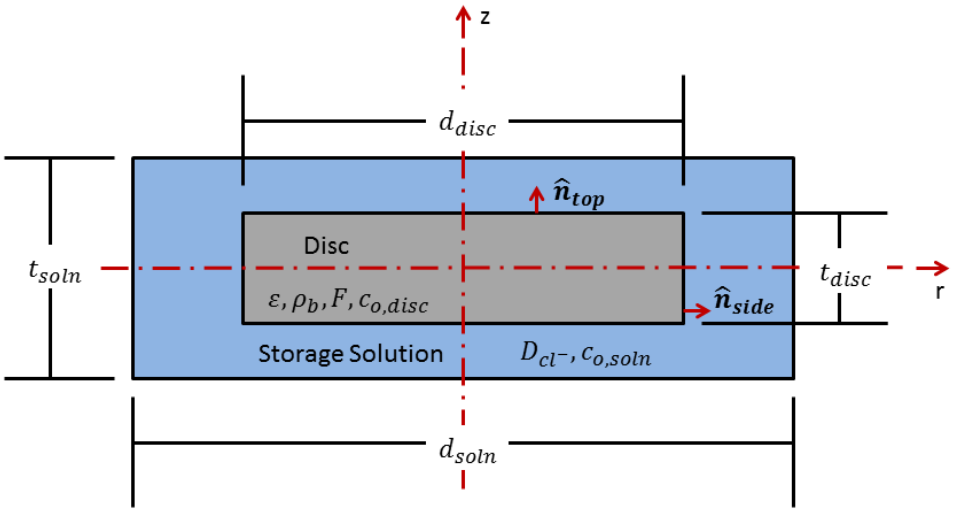

Figure 4 *Schematic of two-dimensional, axis-symmetric domain (coordinates z and r are shown) used in leaching model; the origin of the coordinate system is located at the center of the sample. Taking advantage of the symmetry of the system, only the top right quadrant was modeled.*

In Equation 3, c_i and $\boldsymbol{j_i}$ are the molar concentration and molar flux (moles per unit area of the disk per time) of the i^{th} species, respectively. The molar flux is given by Fick's first law, Equation 4, which includes the formation factor to account for the porosity and tortuosity of the matrix [41], where D_0 is the self-diffusion coefficient of chloride ions in water [15].

$$\boldsymbol{j_i} = -\frac{D_0}{F}\nabla c_i \qquad [4]$$

The sample is assumed to have constant (in time and space) diffusivity, and has its pore space saturated with a solution containing chloride ions; it is assumed that the degree of saturation did not vary in time. The diffusivity in Equation 4, D_0, is related to the porosity, connectivity, and

effective diffusivity through Equation 1. Combining Equations 1, 3, and 4 produces Equation 5 that describes the transport of the ionic species through the disc.

$$\phi \frac{\partial c_i}{\partial t} - \nabla \cdot \left(\frac{D_0}{F} \nabla c_i \right) = 0 \quad [5]$$

Equation 5 also describes the transport of chloride ions through the storage solution with the exception that the formation factor and porosity are set to unity. The self-diffusivity of chloride ions in water used in this study, for 25 °C, was 18.9×10^{-10} m^2/s [15,43].

The computational domain is bounded by the two-dimensional plane at θ=0, and extends throughout the region (0≤r≤R, 0≤z≤Z). The boundary conditions at $z = 0$ and $r = 0$ are given in equations 6a and 6b, respectively. The initial chloride concentration is given by the initial condition given in equation 6c.

$$\frac{\partial c_i}{\partial z}(0, r, t) = 0 \quad [6a]$$

$$\frac{\partial c_i}{\partial r}(z, 0, t) = 0 \quad [6b]$$

$$c_i(z, r, 0) = c_{0,disk} \quad [6c]$$

At the interface of the disc and storage solution, continuity between the molar flux leaving the disc and entering the storage solution is assumed. This condition is expressed in Equation 7 where $\hat{\boldsymbol{n}}_{\boldsymbol{disc}}$ and $\hat{\boldsymbol{n}}_{\boldsymbol{solution}}$ are the outward pointing normal vectors to the surface of the disk and storage solution, respectively. In Figure 4, when the domain of interest is the ceramic disk and

300 the flux through the top surface is computed $\hat{\boldsymbol{n}}_{\boldsymbol{disk}} = \hat{\boldsymbol{n}}_{top}$. When computing the flux through
301 the side surface of the ceramic disk, $\hat{\boldsymbol{n}}_{\boldsymbol{disk}} = \hat{\boldsymbol{n}}_{side}$.
302

$$\boldsymbol{j}_{i,disk} \cdot \hat{\boldsymbol{n}}_{\boldsymbol{disk}} = \boldsymbol{j}_{i,solution} \cdot \hat{\boldsymbol{n}}_{\boldsymbol{solution}} \quad [7]$$

303

304 Equation 5 with boundary and initial conditions (Equation 6) and continuity condition (equation
305 7) were solved over the domain in Figure 4 using the finite element method. An initial time step
306 of 36 s was used and the simulation was run to achieve a total leaching time of 6.48 x 10^5 s (180
307 h).
308

309 The molar flux at the disc-storage solution interface was recorded at each time step. To obtain
310 the number of moles of chloride ions entering the storage solution, the flux was integrated over
311 the top and side surfaces and time as shown in Equation 8. All surface and time integrals were
312 computed in the software package.
313

$$q = \int_{t_1}^{t_2} \iint \boldsymbol{j} \cdot \hat{\boldsymbol{n}}\, dSdt = \int_{t_1}^{t_2} \iint \left(\boldsymbol{j}_{\boldsymbol{side}} \cdot \hat{\boldsymbol{n}}_{\boldsymbol{side}} + \boldsymbol{j}_{\boldsymbol{top}} \cdot \hat{\boldsymbol{n}}_{\boldsymbol{top}}\right) dSdt \quad [8]$$

314

315 Initial simulations produced long term equilibrium storage solution concentrations that, while
316 consistent with a simple mass balance, were not in agreement with the measured experimental
317 values. Subsequent investigations revealed that this difference was due to sorption (binding) of
318 chloride ions by both the ceramic disc and siltstone substrates. Based on this measured sorption,
319 the initial pore solution concentrations were adjusted appropriately in a second set of
320 simulations, producing the modeling results that are provided in the remainder of this paper.

The surface and uniaxial resistivity of the siltstone and concrete cylinders is modeled using a three dimensional (3D) domain. A 2D axi-symmetric model is appropriate to predict the storage solution concentration as the ion concentration inside the specimen varies along the specimen's radius and thickness only. This is not the case for the potential field created during a surface resistivity measurement because there is no axis of symmetry for the surface resistivity test. Figure 5 shows the geometry used for these calculations. Initially, the sample (without the surface or end electrodes) is saturated with a concentrated solution. At predetermined time intervals, the solution concentration in each computation element is used, along with the formation factor, to calculate the bulk conductivity at each element. Electrodes are added to the system (with the appropriate boundary conditions for the current flow) and the bulk response is calculated.

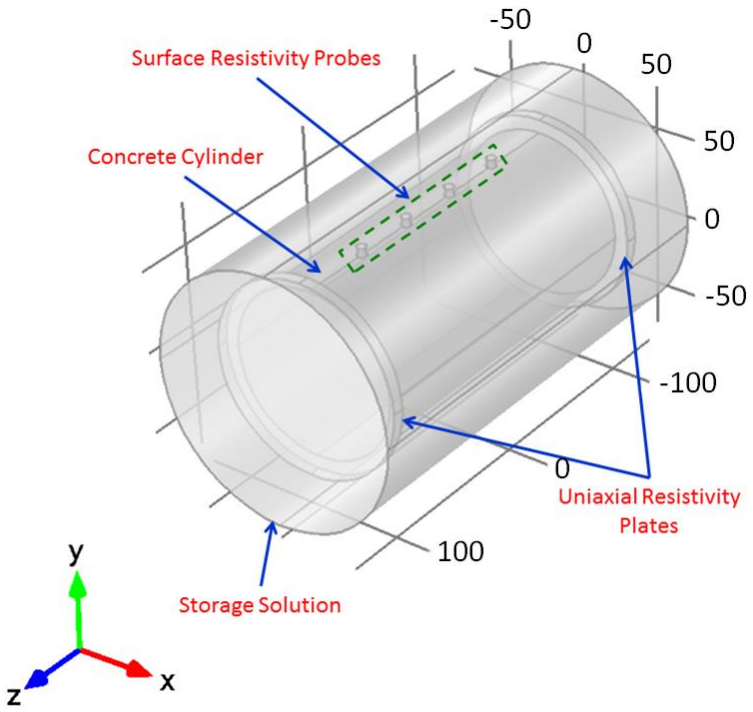

334

335 ***Figure 5*** *3D model used to solve for surface and uniaxial resistivity, dimensions given in mm.*

336

337 When simulating the resistivity measurements, the ion concentration inside the cylinder and the
338 applied voltage potential is important. For the siltstone cylinders, the pore solution is composed
339 of potassium chloride (KCl) dissolved in de-ionized water. The potassium (K^+) and chloride (Cl^-)
340 species contribute to the resistivity calculations and Equation 5 describes their movement
341 through the cylinder. For concrete, hydroxide (OH^-), potassium (K^+), and sodium (Na^+) are the
342 species that contribute to pore solution conductivity and Equation 5 describes their
343 concentration inside the cylinder over time. The model does not assume electro-diffusion effects
344 of multiple ions in the pore solution. It computes ion concentration of each species independent
345 of other ions.

346

Calculating the bulk resistivity required solving for the voltage (Φ) everywhere in the system. To do this, one needs to calculate the current flux $\boldsymbol{I}$ between adjacent computational nodes. The current flux depends upon the electric field ($\boldsymbol{E} = -\nabla\Phi$) and the local conductivity σ:

$$\boldsymbol{I} = \sigma\boldsymbol{E} \qquad [9]$$

The local conductivity is a function of local species concentrations in the solution ($c_i(\boldsymbol{x})$) and the local formation factor:

$$\sigma = \frac{\sigma_{\text{soln}}\left(c_i(\boldsymbol{x})\right)}{F} = \beta\phi\sigma_{\text{soln}}\left(c_i(\boldsymbol{x})\right) \qquad [9]$$

In the storage solution, $\beta = \phi = 1$.

At each point in time during the leaching process, the concentration of the ions in the pore solution is a function of the position inside the cylinder. The ion conductivity is a function of the ion concentration and valence, shown in Equation 12, refer to Snyder et al. [18] for a detailed description of this relationship.

$$\sigma_{\text{soln}} = \sum_{i}^{n} z_i c_i \frac{\lambda_i^o}{1 + G_i\left(1/2\sum_i^n z_i^2 c_i\right)^{1/2}} \qquad [12]$$

The index i represents a particular species and goes from 1 to n species. The quantities z_i and c_i are the species valence and molar concentration, respectively. The values λ_i^o and G_i are the conductivity of the species at infinite dilution and conductivity coefficients (see [18]), respectively.

At each time step in the simulation, Equation 5 determines the ion concentration resulting from the leaching process. The local concentrations are used to solve for the electric potential everywhere. The cylinder resistance is determined in post-processing by computing the current flux through the electrodes (surface probes or end plates). Integrating the current flux over the surface of the electrode is used to calculate the total electrical current. In all simulations a 2 V potential difference is applied (-1 V to 1 V). Applying the appropriate correction factor depending on specimen size and electrode configuration as discussed previously converts the resistance to resistivity.

Figure 6 illustrates the iso-potential surfaces for the surface and uniaxial case of a 100 mm by 200 mm concrete cylinder subjected to leaching for 180 days. At each time-step, the electrode voltages remain the same, but the magnitude of the current flow changes with the changing conductivity.

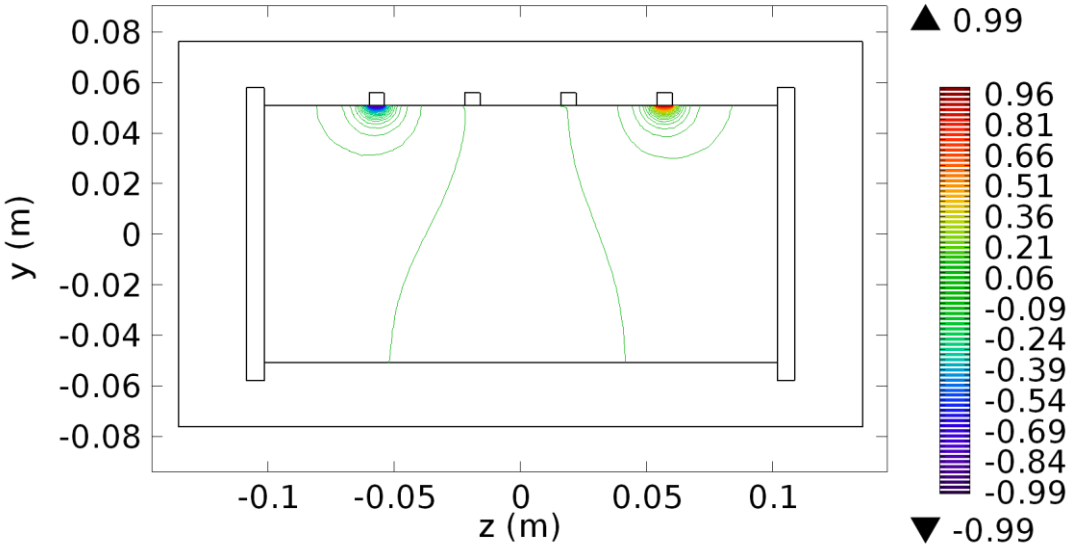

(a)

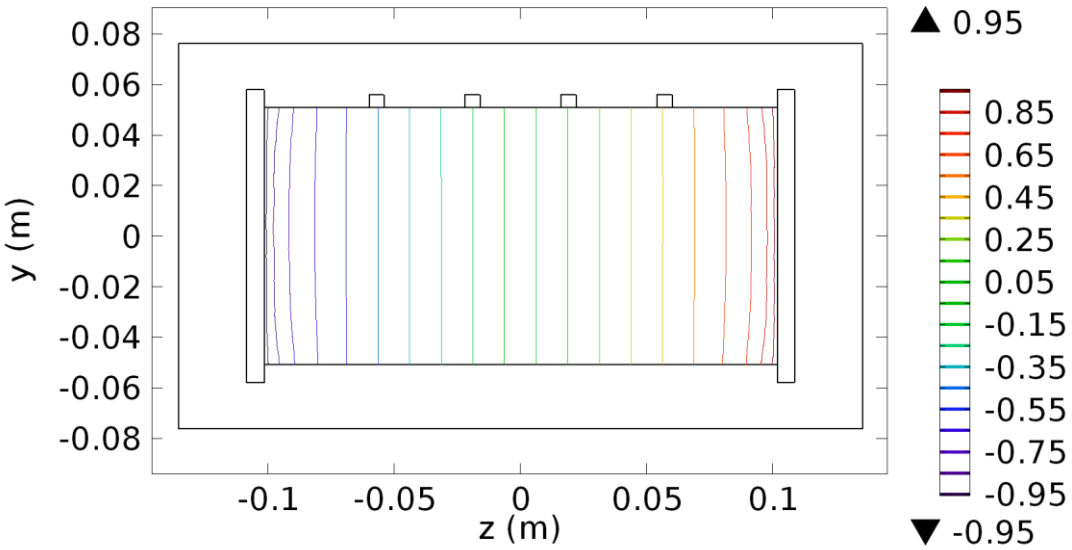

(b)

Figure 6 *Images show lines of constant potential on the y-z plane in side of the concrete cylinder, containing OH-, K+, and Na+ ions, when applying a voltage potential to the a) surface and b) to the ends of the cylinder (uniaxial measurement). The potential lines in (b) are curved near the ends of the cylinder, indicating leaching is occurring from the ends of the cylinder and around its circumference.*

4 Results and Discussion

The results from the three phases of this study are described in detail below.

4.1 Phase I: Leaching Demonstration and Characterization

The objective of Phase I was to demonstrate where leaching of conductive species occurs, a diffusion approach could be used to characterize this process. The ceramic discs were saturated with a solution of KCl, which had an experimentally measured resistivity of 0.135 Ω·m, while the average uniaxial resistivity of the discs was 0.552 Ω·m, which implies a formation factor, $F_{ceramic}$, of 4.1 ± 0.5.

Once the formation factor of the ceramic was determined, the specimens were placed into different containers containing different storage solutions and storage volumes, as described by Figure 2. The storage solution concentration was monitored during the leaching process, and serves as a measure of how the concentration of the storage solution is changing due to ions leaving the ceramic specimen's pore solution and entering the storage solution.

For the specimens placed in the deionized water (Storage Solution A), the initial concentration of the storage solution is zero and increases over time, as shown in Figure 7. As expected, for the larger amount of storage solution surrounding the sample, A5 versus A2, the concentration of the storage solution is lower because the same number of initial ions in the ceramic pore solution must be distributed through a larger total volume of solution (sum of the pores in the ceramic and the volume of storage solution).

For the B series of specimens, the storage solution concentration was chosen to match that of the specimen pore solution, and as expected, the results in Figure 7 indicate that very little

412 transfer of chloride ions between the two solutions occurred. For the C series, the storage
413 solution chloride ion concentration was higher than that of the specimen pore solution and
414 therefore the concentration of the storage solution decreased over time as in this scenario,
415 chloride ions diffused from the higher concentration storage solution into the lower
416 concentration specimen pore solution.
417
418 In general, the agreement between the simulation and the experimental results shown in Figure
419 7 is reasonable with the average error between the measured and simulated concentration
420 ranging between 16 % to 38 % for the A series specimens, 0.5 % to 1.2 % for the B series
421 specimens, and 0.6 % to 1.7 % for the C series specimens. A mass balance can be employed to
422 calculate the expected final equilibrium concentration of the storage solution and this value
423 would agree with the long-term (> 150 h) simulation results shown in Figure 7 case. The long-
424 term (equilibrium) simulation and experimental results are contrasted in Figure 8, where it can
425 be seen that the ratio between the experimental and simulated equilibrium values is
426 approximately one for all storage solution concentrations measured in this study.
427

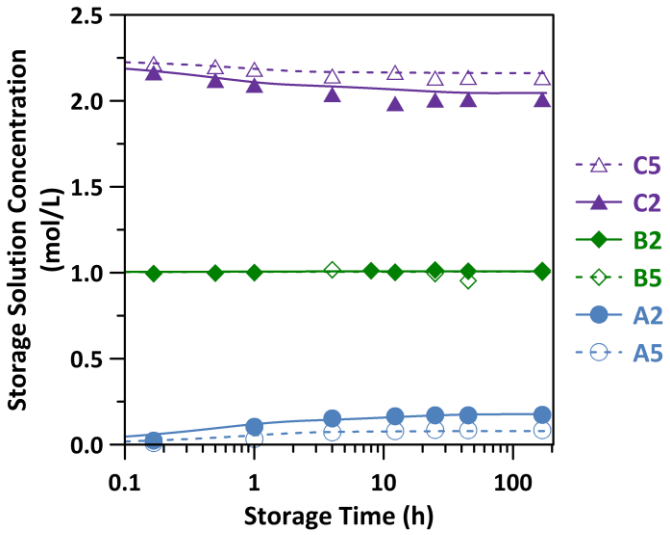

428

429 ***Figure 7*** *Concentration of storage solutions as ceramic specimens saturated with a 1 mol Cl^- / L*

430 *solution leached into storage solutions. The intial concentrations of the storage solutions were*

431 *A) 0.0 mol Cl^- / L; B) 1.0 mol Cl^- / L; and C) 2.25 mol Cl^- / L. Points represent measured*

432 *concentration, while lines represent data simulations. Concentration measurments have a*

433 *coefficient of variation of 1.5 %.*

434

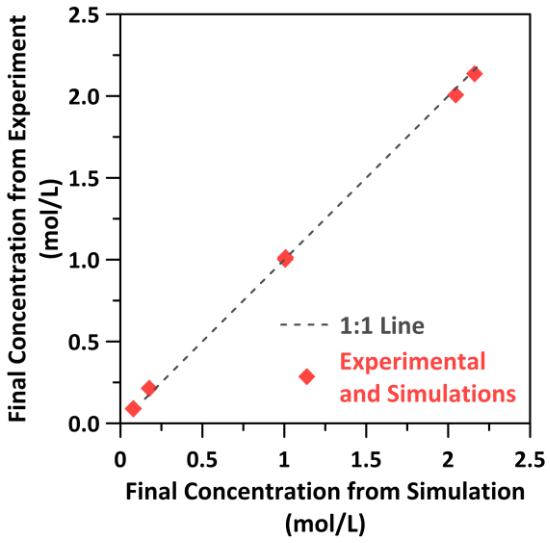

435

436 ***Figure 8*** *Measured and Final concentration of storage solutions as ceramic specimens*
437 *saturated with a 1 mol Cl^- / L solution leached into storage solutions. Points represent measured*
438 *and simulated results, and the dashed-line represents a perfect one-to-one relationship.*
439 *Concentration measurments have a coefficient of variation measurment of 1.5 %.*
440

441 The effect of temperature has also been discussed, as diffusion is a process that is influenced by
442 temperature. As the temperature increases, the diffusion process happens at a faster rate. This
443 is illustrated in Figure 9, by both experimental observations (points) and simulations (lines). The
444 higher temperature (plotted in red and denoted using a suffix of "-45") show that concentrations
445 reach higher values faster in both storage solution to sample ratio systems. This is illustrated by
446 looking at a storage time along the x-axis, and noticing that the higher temperature data is at a
447 higher value. Furthermore, at a sufficiently long storage time, the concentration of both systems
448 approaches the same concentration. Further research is needed to confirm this effect in
449 cementitious systems, as the solubility of different ionic species can change and reaction rates
450 also need to be considered.
451

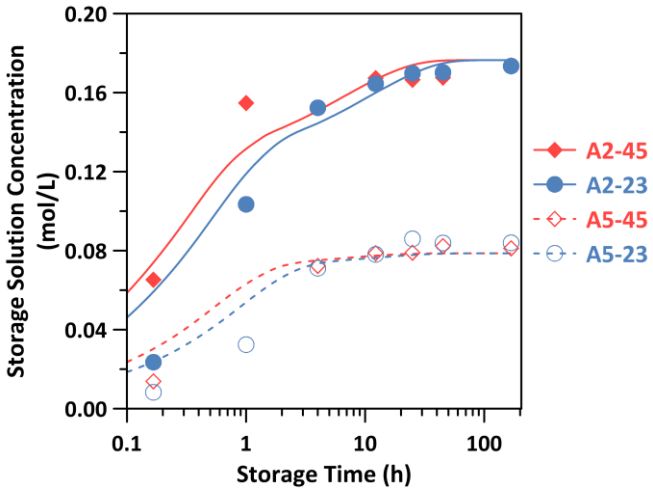

Figure 9 *Concentration of storage solutions for ceramic specimens saturated with a 1 mol Cl- / L solution at temperatures of 23 °C (blue) and 45 °C (red), with different volume of storage solutions (denoted with number following letter). Points represent measured concentration, lines represent data simulations. Concentration measurments have a coefficient of variation of 1.5 %.*

4.2 Phase II: Impact on Electrical Measurements

The objective of Phase II of this study was to illustrate that the leaching of ions in the pore solution can influence the relationship between two different resistivity test geometries, namely uniaxial and surface configurations. Siltstone cores were saturated with KCl solutions, as described in Figure 3. The saturated siltstone cores were placed into solutions of deionized water, and as the leaching process proceeded, the cores were measured for uniaxial and surface resistivity, as shown in Figure 10. The initial resistivity of the cores were divided by the resistivity of the respective pore solutions to determine the average formation factor, $F_{siltstone}$, of 55.2 with a standard deviation of 1.6.

Initially, siltstone specimen 2 had a higher resistivity than specimen 1 because it is saturated with a solution that has a higher resistivity. As the time of leaching increases, both surface and uniaxial resistivity increase, as the ions in the pore solution leach into the surrounding storage solution. The increase in resistivity by a factor of four is only due to increases in the pore solution resistivity as the leaching process happens, while the microstructure remains unchanged. This is one reason that electrical measurements should be interpreted with consideration of the pore solution.

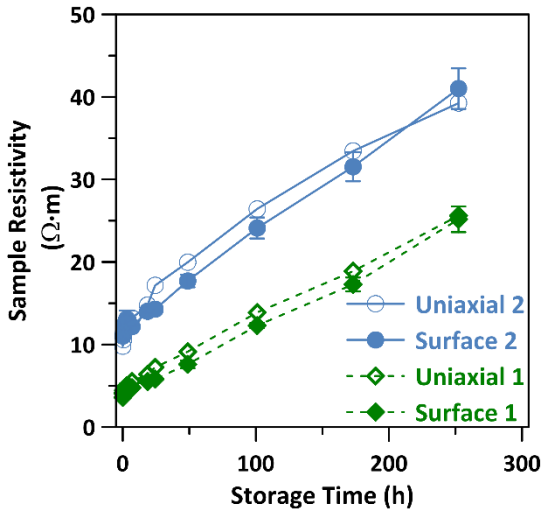

Figure 10 *Measured resistivity for surface or uniaxial geometry for samples saturated in 1) 1.5 mol Cl- / L and 2) 0.5 mol Cl- / L solution and then placed into deionized water for various storage times. Error bars represent one standard deviation from the mean.*

The leaching of the conductive species from the siltstone's pore solution into the surrounding storage solution can create a layered effect in a cylindrical geometry, with the outer "cylindrical shell" in the cylinder consisting of a pore solution of lower ionic concentration than that of the

484 inner core. Using the diffusion approach from Phase I of this study, this layered effect can be
485 quantified in terms of the ionic concentration profile along the radius of cylinder (near the center
486 of the cylinder), shown in Figure 11. As the concentration is normalized, both the higher
487 concentration and lower concentration pore solutions show a similar trend over time.
488

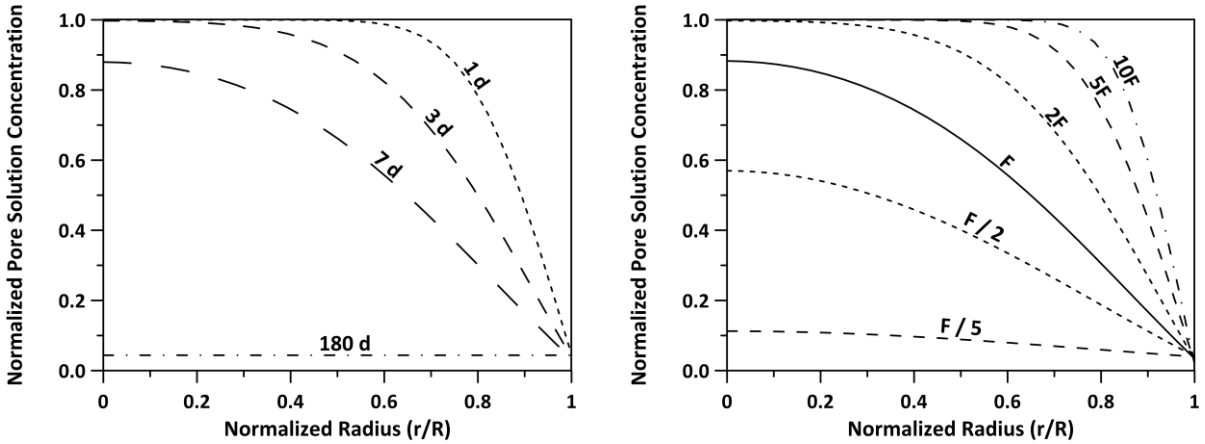

489 ***Figure 11*** *Simulations of pore solution concentration normalized by the concentration before*
490 *leaching for siltstone specimens as function of the normalized radius (where 0 represents the*
491 *core and 1 represents the outside surface) for a) the specimens used in this study at increasing*
492 *leaching times of 1, 3, 7 and 180 d and b) for multiples of the siltstone's formation factor, F =*
493 *55.2, at a leaching time of 7 d.*
494

495 It can be noticed, even at leaching times up to 3 d, the ionic concentration of the pore solution
496 near the center of the cylinder is similar to the initial concentration. However, the concentration
497 near the surface of the specimen drops quite rapidly. At a leaching time of 7 d, the concentration
498 throughout the entire section of the specimen has decreased measurably. At a leaching time of

180 d, the concentration has nearly become uniform at a very low value corresponding to equilibrium with the leaching (storage) solution.

This concentration profile in the radial direction is also influenced by the formation factor of the material, demonstrated in Figure 11b, at an age of 7d. Recall that a higher formation factor represents a less porous material and lower connectivity. The solid curve marked F is using the same formation factor as the siltstone used in this study, 55.2. If the formation factor is decreased, the leaching process happens faster, and the concentration along the radial direction reaches uniformity sooner. Conversely, if the formation factor is increased, the diffusion happens at a slower rate. This creates a higher gradient and also requires a longer time to reach a uniform concentration. It is worth noting, that typical formation factors of regular OPC bridge-deck concretes can be around 500 (or about the 10F line in Figure 11); however, this leaching behavior is still observed, as ion transport is governed by Fick's law with the formation factor only dictating the rate of transport [24].

Previous work has demonstrated how finite layered effects can influence surface and bulk electrical measurements in different ways: half-space [44], or finite slab geometries [11,45–47]. One approach to investigate the effects of layered materials is to study the ratio of surface resistivity to uniaxial resistivity, as originally described by Morris et al. [40]. Recent research has shown that this factor can change as these layered systems evolve [11,48].

Figure 12 presents the ratio of surface resistivity (corrected for geometry according to equation 2) and uniaxial resistivity. The initial experimental and simulation values of the ratio differed slightly (1.12 vs. 0.93), so subsequent measured and simulation values were normalized by the corresponding initial value. The solid points represent experimentally measured values, while the lines represent results from the multiphysics simulation that coupled the diffusion model to obtain the pore solution resistivity gradient and a surface or uniaxial resistivity test. During the initial phase of the leaching process, the ratio decreases. However, after a sufficient amount of time, the ratio begins to increase and again approaches the initial value. This is to be expected because only the initial state and the final steady state are composed of homogeneous (but different) specimens. The specimen during the intermediate phase is relatively heterogeneous, as the leaching of the pore solution leads to an outer core of lower concentration that affects bulk and surface measurements differently. In this experiment, the effect of leaching changed the resistivity ratio by more than 20 %.

While leaching will influence both the uniaxial and surface resistivity, the use of the ratio of surface to uniaxial resistivity appears to be a good method of assessing sample heterogeneity, and the degree to which leaching has happened. It is also important to note that leaching will increase the resistivity of the pore solution in the outer core and will increase both the surface and uniaxial resistivity measurements (shown in Figure 10). For shallow depths of leaching, the ratio of surface to uniaxial resistivity has been shown to be less than unity, mostly due to the large probe spacing that samples the underlying material while the uniaxial resistivity changes more with a more resistive outer layer [45,48–50]. For larger depths of leaching this ratio has

been seen to be higher than unity [48]. When the ratio is close to unity, it can either be assumed that there is no leaching or that sufficient leaching has happened that the material is homogeneous once again. If the ratio differs from 1 by more than 5 %, it can be assumed that leaching is occurring and there is a gradient in the pore solution concentration within the test specimen.

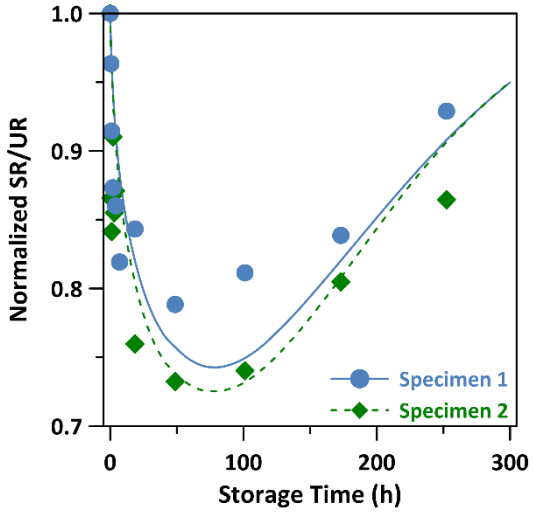

Figure 12 *Ratio of measured surface resistivity to uniaxial resistivity for siltstone specimens saturated with 1) 1.5 mol Cl- / L and 2) 0.5 mol Cl- / L solution and then placed into deionized water for various storage times. Resistivity measurements have a coefficient of variation of ± 4 %.*

4.3 Phase III: Extension to Cementitious Systems

Phase III of this study will provide an estimation of the effects and magnitude of leaching of pore solution on electrical resistivity measurements on cementitious materials. The concrete material that was modeled was a mixture that had a *w/c* of 0.4, made with Type I OPC, with a 91 d formation factor of 420 ± 95 and a porosity of 14.6 % ± 0.5 %, which has been characterized by

Spragg et al. [51]. The initial concentration of the pore solution was calculated based upon the mixture designs, cement chemistry, and degree of hydration using the online calculator discussed previously [19]. The initial concentration of the storage solution was assumed to be zero.

The multiphysics model that was developed in the first section of the paper is able to describe the diffusion of ionic species based upon the formation factor of the material, and the concentrations of the pore and storage solutions. Of particular importance is the concentration along the radius of the concrete cylinder. The concentration of Na^+, K^+, and OH^- can be converted to pore solution resistivity, as described by [18]. These results are shown in Figure 13a for a standard 100 mm x 200 mm cylindrical test specimen and Figure 13b for a standard 150 mm x 300 mm cylindrical test specimen. Figure 13 shows calculated pore solution resistivity as a function of the normalized radius (*r/R*), where zero represents the center of the specimen and unity represents the cylinder surface; the symbols represent calculated quantities and the lines guide the eye.

Figure 13 shows that for this hypothetical case, specimens that begin saturated with a known pore solution and are then placed in a solution of low concentration, can develop a measurable pore solution resistivity gradient within 28 d. Note that only the normalized radius from 0.8 to 1.0 is shown, because the resistivity remains relatively constant closer to the center of the cylinder. The resistivity of the pore solution at the surface of test specimen can range from two to three times higher than that inside of the test cylinder. Furthermore, these results suggest that for both 100 mm and 150 mm diameter test cylinders, the leached depth is about 8 mm. This

580 suggests that if specimens must be water-cured, a 150 mm diameter specimen could be cored to
581 a diameter of 130 mm or less before testing with little worry about leaching within the cut
582 volume, even at a curing period of up to 91 d.

583

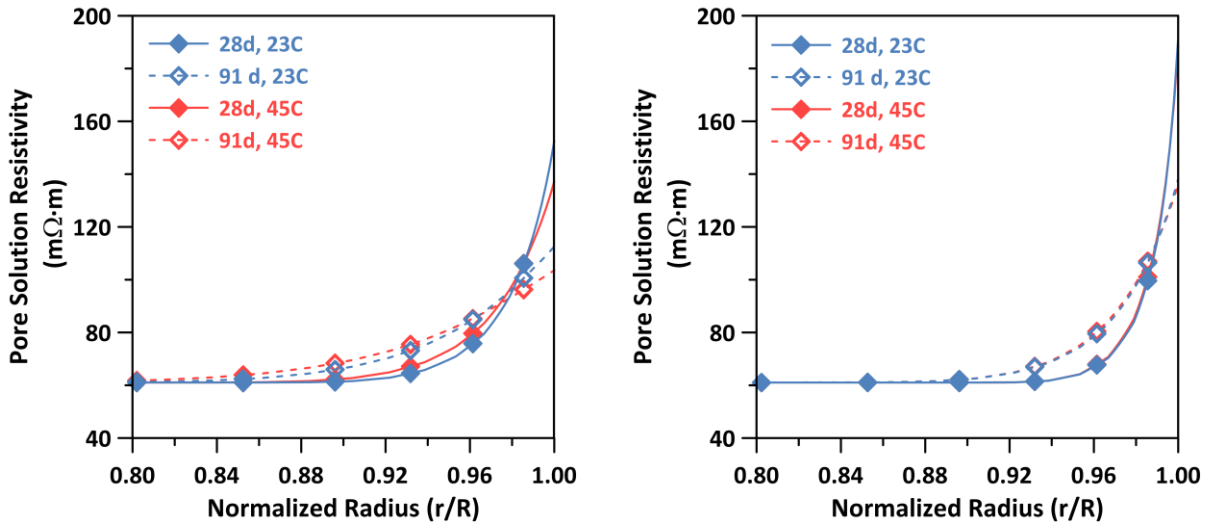

584 ***Figure 13*** *Calculated pore solution resistivity profile at leaching times of 28 and 91 d, at*
585 *conditioning temperatures of 23 °C and 45 °C, for a) standard 100 mm x 200 mm cylindrical test*
586 *specimen and b) standard 150 mm x 300 mm cylindrical test specimen. Resistivity*
587 *measurements have a coefficient of variation of ± 4 %.*

588

589 The gradient shown in Figure 13 will influence resistivity measurements, especially surface
590 resistivity measurements that are sensitive to surface conditions [45,48]. This effect was
591 investigated for each time step using the corresponding gradient, similar to that shown in Figure
592 13 for 28 d and 91 d, with the second part of the multiphysics model that is able to compare
593 uniaxial and surface resistivity measurements.

594

595 The results, shown in Figure 14, illustrate that at a zero leaching time, the ratio of surface to
596 uniaxial resistivity is 0.95, and as the specimen leaches the ratio will decrease. This ratio will reach
597 a minimum (at a point when the specimen has become the most heterogeneous). The value will
598 increase, eventually reaching a value of 1 as the system becomes homogeneous (albeit with a
599 lower pore solution concentration). The specimen at the higher temperature reaches its
600 maximum leached point, the minimum of the dashed line in Figure 14, at an earlier leaching time.
601 The leaching specimen at the higher temperature also has a SR /UR that approaches its initial
602 value at faster rate, which is expected as the higher temperature causes diffusion to occur at a
603 faster rate within the multiphysics model.

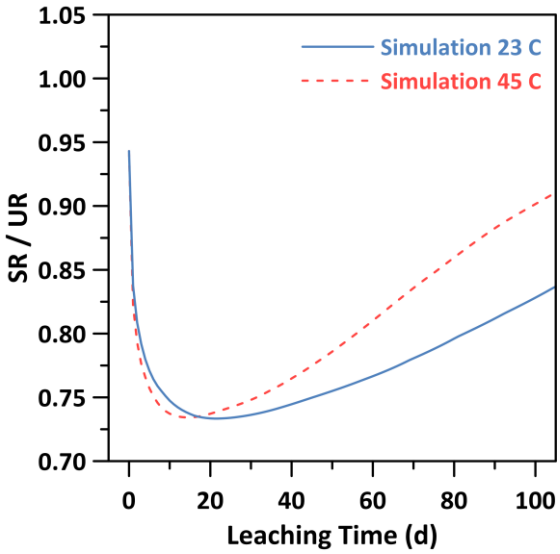

604

605 ***Figure 14*** *Ratio of surface to uniaxial resistivity for 100 mm x 200 mm cylindrical specimens*
606 *submerged in tap water at an age of 91 d as the leaching time increases for two different*
607 *temperatures.*

608 It should be highlighted that both Figure 13 and Figure 14 represent a purely hypothetical case.
609 Specifically, the concrete specimen starts out completely saturated with a known solution, the
610 formation factor remains constant over the leaching period, and there are no binding effects.

611 This can be contrasted with typical concrete curing practice, which is to place the specimen in a
612 storage solution consisting of lime saturated water from an early age. For this real life scenario,
613 the previous assumptions do not hold. Specifically, with specimen age: the pore solution is
614 changing concentration due to both leaching and hydration, the formation factor is changing
615 (often several orders of magnitude) due to pore refinement that accompanies hydration of the
616 cementitious materials, and there are changes in the alkali binding behavior of these materials
617 with changes in temperature and degree of hydration. The point being, experimental data that
618 matches the model data is difficult to obtain.
619
620 Experimental data presented here is designed to match typical concrete industry curing practices,
621 consequently, the experimental and model data are not directly comparable. However, the
622 conclusions from the experimental data are drawn based on similarities from the model results.
623 Experimental results from concrete specimens, shown in Figure 15, show the ratio of surface to
624 uniaxial resistivity for cylindrical 100 mm x 200 mm concrete specimens that were placed into
625 sealed conditions or lime saturated water at an age of 1 d, at (23 ± 1) °C. After 7 d of curing at (23
626 ± 1) °C to allow for microstructure development, half of the specimens cured in lime saturated
627 water were placed at (45 ± 1) °C. The specimens were monitored as they aged in their respective
628 curing conditions.
629
630 The concrete specimens that are cured under sealed conditions maintain a ratio very close to 1.0,
631 which suggests that no significant leaching takes place in specimens that are sealed cured. Similar
632 results have been observed by Bentz et al. [52] for specimens cured in a 98 % RH environment,

633 i.e. a moist room. Their data show good agreement between surface and uniaxial resistivity
634 measurements, at ages of 1 d, 7 d, 28 d, and 90 d for a variety of OPC and high-volume fly ash
635 concretes. This is logical, as in both of these cases there is no surrounding storage solution with
636 a significantly lower alkali concentration that drives the leaching of alkalis.
637
638 However, moist cured specimens exhibit a decrease in the SR / UR. Specimens that are lime water
639 cured at 23 °C for their entire life, exhibit an initial value close to 1.0 which decreases over time,
640 but eventually will increase again as the specimen experiences sufficient leaching. The SR / UR
641 does not reach as low a value as in the simulations, as the leaching process is occurring
642 concurrently with the decrease in pore solution resistivity due to hydration, and results in a
643 smaller gradient compared to that predicted in the model. The specimens cured at 45 °C exhibit
644 this decrease in SR / UR which is indicative of leaching, but will reach a lower ratio than the
645 specimens cured at 23 °C. This can be due to the elevated temperature increasing the hydration
646 rate, which decreases the resistivity of the pore solution in the inner core, while the increased
647 leaching rate results in a higher resistivity of the pore solution on the outer edge of the specimen.
648 Again, the SR / UR approaches 1.0 for long leaching times.
649

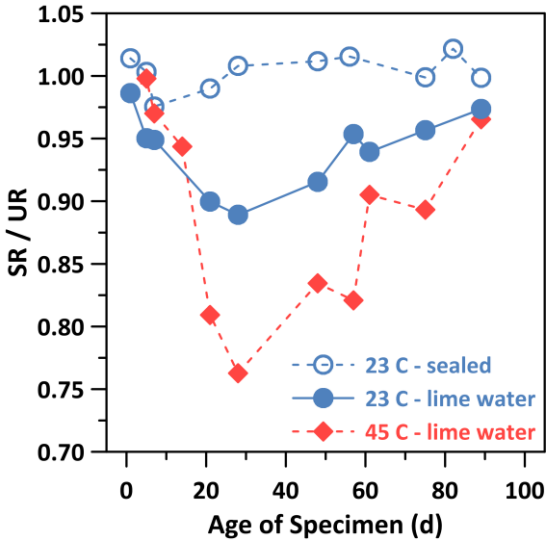

650

651 ***Figure 15*** *Ratio of experimental surface to uniaxial resistivity for 100 mm x 200 mm cylindrical*
652 *specimens lime-water cured and sealed cured described by Spragg* [11] *on concrete specimens*
653 *as they age. Resistivity measurements have a coefficient of variation of ± 4 %.*

654

655 **5 Summary and Conclusions**

656 Electrical measurements are gaining interest in the concrete industry as a rapid method of
657 characterizing the microstructure. These measurement methods, when combined with
658 information about the pore solution resistivity, can yield information about the specimen
659 diffusivity. This is largely attributed to the use of the Nernst-Einstein relationship, which relates
660 the measured resistivity to ion diffusion coefficients. However, proper information is needed
661 regarding the pore solution resistivity. Previous research has demonstrated that there are
662 dependencies on the volume of storage solution surrounding the specimens [24] and the type of
663 storage solution [11]. These dependencies have been attributed to the leaching of the conductive
664 ionic species from the pore solution.

665

This study has investigated the leaching of conductive species from a pore solution into the surrounding storage solution. The study began by demonstrating that ionic leaching occurs, with the use of ceramic disks. The specimens were saturated with solutions of potassium chloride, and were placed into storage solutions of different volumes and different concentrations. Results indicate that the volume and concentration of the storage solution and the conditioning temperature will influence the rate of leaching, which is primarily related to the difference in ionic concentration between the pore and storage solutions. Furthermore, it was demonstrated through numerical simulations that microstructural properties (formation factor) can be used to characterize the rate of leaching.

The second phase of this study utilized cores of siltstone to demonstrate that the leaching of the ionic species can influence electrical measurements and even how different measurements (surface and uniaxial resistivity in this study) are related. An increase in specimen resistivity was observed, which was attributed purely to the leaching of the ionic species. Furthermore, the ratio of surface to uniaxial resistivity, which has been employed to indicate material homogeneity by Spragg [11], was shown to decrease as the leaching happens, but after sufficient leaching the value once again approach the initial value near 1. This suggests that after a sufficient amount of leaching, the material is again homogeneous, but the pore solution is much less concentrated than it was initially. The use of this resistivity ratio may be an effective way of evaluating the presence of on-going leaching.

The effects of leaching on electrical measurements on cementitious materials were discussed through the use of a diffusion model. Without consideration of binding or dissolution, and considering the storage solution as similar to tap water, the pore solution resistivity was estimated to increase up to three times its original value, and the ratio of the surface resistivity to the bulk resistivity decreased by as much as 10 % at room temperature.

In conclusion, this study has demonstrated that the leaching of ionic species occurs when samples are immersed in a fluid during curing and can drastically influence electrical measurements. The influence of these effects needs more evaluation for the impact on acceptance measurements for concrete projects, but their effects should be considered in current evaluations and in future standardization efforts. Methods such as moist-room curing could reduce the leaching (research has suggested that leaching can occur due to the water that condenses on the surface of a specimen in a moist room) or sealed curing would eliminate leaching [11,29]. However, additional corrections could be needed for the degree of saturation [22]. Additionally, these concretes (e.g., sealed cured or cured in a moist room) have exhibited good agreement between surface and uniaxial resistivity measurements at ages of 1 d, 7 d, 28 d, and 90 d for a variety of OPC and high-volume fly ash concretes [11,52].

6 Acknowledgements

This work was supported in part by the Joint Transportation Research Program administered by the Indiana Department of Transportation and Purdue University (Project SPR 3708). The contents of this paper reflect the views of the authors, who are responsible for the facts and the

accuracy of the data presented herein, and do not necessarily reflect the official views or policies of the Federal Highway Administration and the Indiana Department of Transportation, nor do the contents constitute a standard, specification, or regulation. The authors would like to acknowledge helpful discussions from Professor Sidney Diamond and Professor Farshad Rajabipour.

7 References

[1] W.J. McCarter, M.C. Forde, H.W. Whittington, Resistivity Characteristics of Concrete., ICE Proc. 71 (1981) 107–117. doi:10.1680/iicep.1982.1993.

[2] E.J. Garboczi, Permeability, diffusivity, and microstructural parameters: A critical review, Cem. Concr. Res. 20 (1990) 591–601. doi:10.1016/0008-8846(90)90101-3.

[3] C. Andrade, Calculation of chloride diffusion coefficients in concrete from ionic migration measurements, Cem. Concr. Res. 23 (1993) 724–742. doi:10.1016/0008-8846(93)90023-3.

[4] W. Elkey, E. Sellevold, Portland Cement Concrete Pavement Permeability Performance, Directorate of Public Roads, Norwegian Road Research Laboratroy, Oslo, 1995.

[5] R.B. Polder, Test methods for on site measurement of resistivity of concrete - a RILEM TC-154 technical recommendation, Constr. Build. Mater. 15 (2001) 125–131. doi:10.1016/S0950-0618(00)00061-1.

[6] R. Kessler, R. Powers, M. Paredes, Resistivity Measurements of Water Saturated Concrete as an Indicator of Permeability, in: NACE International, 2005.

[7] A.A. Ramezanianpour, A. Pilvar, M. Mahdikhani, F. Moodi, Practical evaluation of relationship between concrete resistivity, water penetration, rapid chloride penetration and compressive strength, Constr. Build. Mater. 25 (2011) 2472–2479. doi:10.1016/j.conbuildmat.2010.11.069.

[8] L. Tang, L. Nilsson, B.P. Basheer, Resistance of concrete to chloride ingress: testing and modelling, Spon Press, London ; New York, 2012.

[9] T.T. Rupnow, P. Icenogle, Evaluation of Surface Resistivity Measurements as an Alternative to the Rapid Chloride Permeability Test for Quality Assurance and Acceptance, Louisiana Department of Transportation, Baton Rouge, LA, LA, 2011.

[10] K.A. Snyder, The relationship between the formation factor and the diffusion coefficient of porous materials saturated with concentrated electrolytes : theoretical and experimental considerations, Concr. Sci. Eng. 3 (2001) 216–224.

[11] R.P. Spragg, The Rapid Assessment of Transport Properties of Cementitious Materials Using Electrical Methods, MSCE, Purdue University, 2013.

[12] N.S. Berke, M.C. Hicks, Estimating the life cycle of reinforced concrete decks and marine piles using laboratory diffusion and corrosion data, in: V. Chaker (Ed.), Corros. Forms Control Infrastructure, ASTM STP 1137, ASTM International, Philadelphia, Pennsylvania, 1992: pp. 207–231.

[13] X. Feng, E. Garboczi, J. Bullard, D.P. Bentz, K. Snyder, P. Stutzman, T. Mason, Expanding a tool for predicting chloride diffusivity in concrete so it can be used by manufacturers to evaluate the durability of concrete made with blended cements. Part I: Characterizing blended cement materials., Gaithersburg, MD, 2004.

[14] E. Garboczi, D.P. Bentz, K. Snyder, N. Martys, P. Stutzman, C. Ferraris, J. Bullard, An electronic monograph: MODELING AND MEASURING THE STRUCTURE AND PROPERTIES OF CEMENT-BASED MATERIALS, Gaithersburg, MD, 2011.

[15] L. Yuan-Hui, S. Gregory, Diffusion of ions in sea water and in deep-sea sediments, Geochim. Cosmochim. Acta. 38 (1974) 703–714. doi:10.1016/0016-7037(74)90145-8.

[16] F. Rajabipour, Insitu electrical sensing and material health monitoring in concrete structures, PhD, Purdue University, 2006.

[17] H.F.W. Taylor, A method for predicting alkali ion concentrations in cement pore solutions, Adv. Cem. Res. 1 (1987) 5–17. doi:10.1680/adcr.1987.1.1.5.

[18] K. Snyder, X. Feng, B. Keen, T. Mason, Estimating the electrical conductivity of cement paste pore solutions from OH^- , K^+ and Na^+ concentrations, Cem. Concr. Res. 33 (2003) 793–798.

[19] D.P. Bentz, A virtual rapid chloride permeability test, Cem. Concr. Compos. 29 (2007) 723–731. doi:10.1016/j.cemconcomp.2007.06.006.

[20] M.R. Nokken, R.D. Hooton, Using pore parameters to estimate permeability or conductivity of concrete, Mater. Struct. 41 (2007) 1–16. doi:10.1617/s11527-006-9212-y.

767 [21] N. Olsson, V. Baroghel-Bouny, L.O. Nilsson, M. Thiery, Non-saturated ion diffusion in
768 concrete - A new approach to evaluate conductivity measurements, Cem. Concr. Compos.
769 40 (2013) 40–47. doi:10.1016/j.cemconcomp.2013.04.001.

770 [22] R. Spragg, Y. Bu, K.A. Snyder, D.P. Bentz, J. Weiss, Electrical Testing of Cement-Based
771 Materials: Role of Testing Techniques, Sample Conditioning, and Accelerated Curing,
772 Purdue University, West Lafayette, Indiana, 2013. doi:10.5703/1288284315230.

773 [23] I. De La Varga, Increased Fly Ash Volume and Internal Curing in Concrete Structures and
774 Pavements, PhD, Purdue University, 2013.

775 [24] R. Spragg, C. Villani, K. Snyder, D.P. Bentz, J.W. Bullard, J. Weiss, Factors That Influence
776 Electrical Resistivity Measurements in Cementitious Systems, Transp. Res. Rec. J. Transp.
777 Res. Board. 2342 (2013) 90–98. doi:10.3141/2342-11.

778 [25] J. Weiss, K. Snyder, J. Bullard, D.P. Bentz, Using a Saturation Function to Interpret the
779 Electrical Properties of Partially Saturated Concrete, J. Mater. Civ. Eng. 25 (2013) 1097–
780 1106. doi:10.1061/(ASCE)MT.1943-5533.0000549.

781 [26] Y. Bu, J. Weiss, The influence of alkali content on the electrical resistivity and transport
782 properties of cementitious materials, Cem. Concr. Compos. 51 (2014) 49–58.
783 doi:10.1016/j.cemconcomp.2014.02.008.

784 [27] AASHTO TP95-11, Standard Method of Test for Surface Resistivity Indication of Concrete's
785 Ability to Resist Chloride Ion Penetration, American Association of State Highway and
786 Transportation Officials, Washington, D.C., 2011.

787 [28] R. Blanks, H. Meissner, The Expansion Test as a Measure of Alkali-Aggregate Reaction, J.
788 Am. Concr. Inst. 42 (1946) 517–540.

789 [29] C. Rogers, R. Hooton, Reduction in Mortar and Concrete Expansion with Reactive
790 Aggregates Due to Alkali Leaching, Cem. Concr. Aggregates. 13 (1991) 42.
791 doi:10.1520/CCA10548J.

792 [30] C. Famy, K.L. Scrivener, A. Atkinson, A.R. Brough, Influence of the storage conditions on
793 the dimensional changes of heat-cured mortars, Cem. Concr. Res. 31 (2001) 795–803.
794 doi:10.1016/S0008-8846(01)00480-X.

795 [31] M. Thomas, B. Fournier, K. Folliard, J. Ideker, M. Shehata, Test methods for evaluating
796 preventive measures for controlling expansion due to alkali-silica reaction in concrete,
797 Cem. Concr. Res. 36 (2006) 1842–1856. doi:10.1016/j.cemconres.2006.01.014.

[32] P. Rivard, M. a. Bérubé, J.P. Ollivier, G. Ballivy, Decrease of pore solution alkalinity in concrete tested for alkali-silica reaction, Mater. Struct. 40 (2007) 909–921. doi:10.1617/s11527-006-9191-z.

[33] Muberra, F.P. Glasser, Long-term leaching mechanisms of Portland cement-stabilized municipal solid waste fly ash in carbonated water, Cem. Concr. Res. 29 (1999) 179–186. doi:10.1016/S0008-8846(98)00194-X.

[34] S. Diamond, Relevance of laboratory studies on delayed ettringite formation to DEF in field concretes, Cem. Concr. Res. 30 (2000) 1987–1991. doi:10.1016/S0008-8846(00)00390-2.

[35] C. Villani, R. Spragg, M. Pour-Ghaz, J. Weiss, The influence of pore solutions properties on drying in cementitious materials, J. Am. Ceram. Soc. 97 (2014) 386–393. doi:10.1111/jace.12604.

[36] C. Di Bella, Chloride transport and shrinkage of plain and internally cured concrete, MS, Purdue University, 2012.

[37] Y. Bu, R. Spragg, J. Weiss, Comparison of the Pore Volume in Concrete as Determined Using ASTM C642 and Vacuum Saturation, Adv. Civ. Eng. Mater. 3 (2014). doi:10.1520/ACEM20130090.

[38] B.J. Christensen, T. Coverdale, R.A. Olson, S.J. Ford, E.J. Garboczi, H.M. Jennings, T.O. Mason, Impedance Spectroscopy of Hydrating Cement-Based Materials: Measurement, Interpretation, and Application, J. Am. Ceram. Soc. 77 (1994) 2789–2804. doi:10.1111/j.1151-2916.1994.tb04507.x.

[39] R.P. Spragg, J. Castro, T. Nantung, M. Paredes, W.J. Weiss, Variability Analysis of the Bulk Resistivity Measured Using Concrete Cylinders, Adv. Civ. Eng. Mater. 1 (2012) 104596. doi:10.1520/ACEM104596.

[40] W. Morris, E.I.I. Moreno, A.A. Sagüés, Practical evaluation of resistivity of concrete in test cylinders using a Wenner array probe, Cem. Concr. Res. 26 (1996) 1779–1787. doi:10.1016/S0008-8846(96)00175-5.

[41] J. Bear, Dynamics of Fluids in Porous Media, Dover, New York, 1975. doi:10.1097/00010694-197508000-00022.

[42] R.B. Bird, W.E. Stewart, E.N. Lig, E.N. Lightfoot, Transport Phenomena, J. Wiley, New York, 2013.

[43] R. Mills, V.M.M. Lobo, Self Diffusion in Electrolyte Solutions: A Critical Examination of Data Compiled from the Literature, Elsevier ; Distributors for the U.S. and Canada, Elsevier Science Pub. Co, Amsterdam ; New York : New York, NY, U.S.A, 1989.

[44] H. Mooney, E. Orellana, H. Pickett, L. Tornheim, A Resistivity Computation Method for Layered Earth Models, Geophysics. 31 (1966) 192–203.

[45] S.G. Millard, K.R. Gowers, Resistivity Assessment of in-Situ Concrete: the Influence of Conductive and Resistive Surface Layers., Proc. ICE - Struct. Build. 94 (1992) 389–396. doi:10.1680/istbu.1992.21502.

[46] S. Millard, Reinforced Concrete Resistivity Measurement Techniques., Proc. Inst. Civ. Eng. Part 2. 91 (1991) 71–88.

[47] Y. Liu, Experiments and Modeling on Resistivity of Multi-Layer Concrete With and Without Embedded Rebar, Florida Atlantic University, 2008.

[48] R. Spragg, C. Villani, J. Weiss, A. Pourasee, S. Jones, D.P. Bentz, K. Snyder, Surface and Uniaxial Electrical Measurements on Layered Cementitious Composites Having Cylindrical and Prismatic Geometries, in: Proc. 4th Int. Conf. Durab. Concr. Struct., Purdue University, West Lafayette, IN, 2014: pp. 317–326. doi:10.5703/1288284315417.

[49] B.P.S. Rathor, H.S. Rathor, A resistivity computation method for layered earth models with transition boundary, Pure Appl. Geophys. PAGEOPH. 85 (1971) 153–160. doi:10.1007/BF00875405.

[50] R.T. Coverdale, H.M. Jennings, E.J. Garboczi, An improved model for simulating impedance spectroscopy, Comput. Mater. Sci. 3 (1995) 465–474. doi:10.1016/0927-0256(95)00005-B.

[51] R. Spragg, C. Villani, J. Weiss, Electrical Properties of Cementitious Systems : Formation Factor Determination and the Influence of Conditioning Procedures, Adv. Civ. Eng. Mater. 5 (2016). doi:10.1520/ACEM20150035.

[52] D.P. Bentz, S.Z. Jones, K.A. Snyder, Design and performance of ternary blend high-volume fly ash concretes of moderate slump, Constr. Build. Mater. 84 (2015) 409–415. doi:10.1016/j.conbuildmat.2015.03.082.